Biomaterials Science

Interplay of nanointerface curvature and calcium binding in weak polyelectrolytes coated nanoparticles

Journal:	*Biomaterials Science*
Manuscript ID	BM-ART-02-2018-000135.R1
Article Type:	Paper
Date Submitted by the Author:	01-Mar-2018

Complete List of Authors:	Nap, Rikkert; Northwestern University, Department of Biomedical Engineering Gonzalez Solveyra, Estefania; Northwestern University, Department of Biomedical Engineering, Department of Chemistry and Chemistry of Life Processes Institute Szleifer, Igal; Northwestern University, Department of Biomedical Engineering

Journal Name

ARTICLE TYPE

Cite this: DOI: 10.1039/xxxxxxxxxx

Interplay of nanointerface curvature and calcium binding in weak polyelectrolytes coated nanoparticles †

Rikkert J. Nap,[a] Estefania Gonzalez Solveyra,[a] and Igal Szleifer*[a]

Received Date
Accepted Date

DOI: 10.1039/xxxxxxxxxx

www.rsc.org/journalname

When engineering nanomaterials for applications in biological systems, it is important to understand how multivalent ions, such as calcium, affect the structural and chemical properties of the polymer-modified nano-constructs. In this work, a recently developed molecular theory was employed to study the effect of surface curvature on the calcium-induced collapse of end-tethered weak polyelectrolytes. In particular, we focused on cylindrical and spherical nanoparticles coated with poly(acrylic acid) in the presence of different amounts of Ca^{2+} ions. We describe the structural changes that grafted polyelectrolytes undergo as a function of calcium concentration, surface curvature, and morphology. The polymer layers collapse in aqueous solutions that contain sufficient amounts of Ca^{2+} ions. This collapse, due to the formation of calcium bridges, is not only controlled by the calcium ion concentration but also strongly influenced by the curvature of the tethering surface. The transition from a swollen to a collapsed layer as function of calcium concentration broadens and shifts to lower amounts of calcium ions as function of radius of cylinder and sphere. The results show how the interplay between calcium binding and surface curvature governs the structural and functional properties of the polymer molecules. This would directly impact the fate of weak polyelectrolytes coated nanoparticles in biological environments, in which calcium levels are tightly regulated. Understanding such interplay would also contribute to rational design and optimization of smart interfaces with applications in, e.g., salt-sensitive and ion-responsive materials and devices.

1 Introduction

Calcium ions are of fundamental biological interest given the vital role that they have in the physiology and biochemistry of living organisms. They are involved in many biology processes. For instance, calcium ions are important signaling molecules.[1] They are one of the most common second messengers in a number of signaling pathways. Calcium ions play an important roll in apoptosis,[2] muscle contraction,[3] chromatin condensation[4], and neuron signaling[5]. From a structural point of view, calcium ions are also important, because they are a component of the cell membrane and are essential for biomineralization.[6] Hence, when envisioning nanomaterials for biomedical applications, it is key to understand how calcium ions interact with all constituent of the nano-construct and what are the designs implications regarding molecular organization and function.

Polymer-coated nanoparticles of different morphologies have been developed for biomedical applications ranging from imaging contrast agents to delivery platforms for therapeutics.[7,8] Of particular interest is the use of nanomaterials engineered with stimuli-responsive, or 'smart', polymers in applications such as drug delivery, tissue engineering, bioseparations, sensors, and imaging.[9,10] These materials respond to external stimuli such as temperature, pH, light, electric field, and chemicals species. For the particular case of calcium, given its ubiquity in biological environments, changes induced by calcium concentrations could provide another stimuli for smart nano-constructs. Therefore, it is

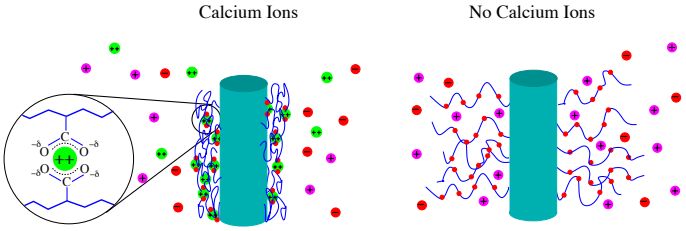

Fig. 1 A schematic representation of the system of study illustrating the effect that calcium ions can have on the structure of the polyelectrolyte layer. The inset shows a calcium bridged complex of two carboxylic acid monomers associated with one calcium ion.

[a] *Department of Biomedical Engineering, Department of Chemistry, and Chemistry of Life Processes Institute, Northwestern University, Evanston, Illinois, USA, E-mail: igalsz@northwestern.edu*

† Electronic Supplementary Information (ESI) available: Details on the total free energy, numerical methodology, and additional results are given. See DOI: 10.1039/b000000x/

important to understand how multivalent ions, such as calcium ions, affect the structural and thermodynamic properties of these polymer-modified nano constructs. Such an understanding is key to optimizing their function, leading to a more rational design of new functional smart materials.

Experimental and theoretical studies of end-tethered (weak) polyelectrolytes have primarily focused on behavior in monovalent electrolyte solutions and a fairly well understood picture has emerged.[11–17] Conversely, the behavior of end-tethered polyelectrolytes in multivalent solutions is less well studied and understood. Experimentally, end-tethered polyelectrolytes undergo a relatively sharp decrease in layer thickness when multivalent ions are added.[18–25] For example, Ezhova and Huber[18] showed that for spherical colloids modified with polyacrylic acid (pAA) brushes in aqueous solutions containing multivalent Mg^{2+} or Ca^{2+} ions, the polymer layer can contract leading the colloids to aggregate. For instance, polyacrylic acid solutions precipitate once a critical calcium ion concentrations is exceeded. Previous theoretical and simulation studies focused on the behavior of strong polyelectrolytes, whose degree of deprotonation is fixed and not influenced by pH, contrary to weak polyelectrolytes whose charge is pH dependent. These studies have proposed and identified various mechanisms for the observed collapse of the polyelectrolyte layer.[21,26–36] Namely, a decrease in osmotic pressure, counter-ion condensation, multivalent ion bridging, and solvophobic effect. The exchange of multiple monovalent ions by one multivalent ion results in a decrease osmotic pressure causing the polymer layer to collapse. Counterion condensation lowers the effective charge of the layer, which results in less stretched chain conformations. This leads to a reduction in the layer thickness. However, the osmotic pressure reduction and counterion condensation it not sufficient to completely describe the observed abrupt collapse.[29] Also, experimental evidence indicates that pAA solutions precipitate in calcium solutions at a ratio of two acid monomers to one calcium ion. This suggest that calcium bridges, i.e., formation of complexes of one calcium with two acid monomers, occur and are an important factor in the collapse of polyelectrolyte brushes. Recently, theoretical studies using a Flory-like approach[29] and Molecular Dynamics simulations[35] showed that the formation of multivalent bridges contributes significantly to the collapse of strong polyelectrolyte layers. Theoretical modeling conducted in our group for pAA-coated spherical nanoparticles, showed that the layers collapse in solutions containing sufficient amounts of calcium given the large propensity to form calcium bridges.[37] The structural collapse of pAA layers was found to be not only dependent on the Ca^{2+} concentration, but also critically influenced by the solution pH and monovalent (NaCl) salt concentration.

So, envisioning applications of weak polyelectrolyte-coated nanoparticles in biological environments requires a profound understanding on how calcium ions interact with the grafted polymers and how this impacts in the resulting molecular organization and chemical state of the polymer chains. Their fate in biological environments lays between the surface of the engineered nanomaterial and surrounding components (ions, proteins, cell membranes, nucleic acids, antibodies, etc.) it encounters. Our goal in this work is to gain understanding on the interplay between the competitive calcium ion binding to end-tethered weak polyelectrolytes and the curvature of the underlying grafting surface under relevant physiological conditions (pH = 7.4 and NaCl salt concentrations of 150 mM). To that end, we theoretically study the calcium-induced collapse of pAA polymers end-grafted to cylindrical surfaces of different radii, as schematically depicted in Fig. 1. We examine the structural organization of the layer and how it changes for calcium concentrations in the range of extracellular media. We also analyze the stability of the polymer layer in terms of the chemical potential of the polymers. Our results show how the interplay between calcium binding and surface curvature governs the structural and functional properties of the polymer molecules. These results are particularly relevant for engineering modified nanoparticles for biological environment, in which calcium concentration changes in the range from nanomolar to micromolar (for cytoplasm and extracellular surrounding respectively)

2 Theoretical Approach

The theoretical approach we employed here is based on a detailed molecular theory that takes into account the size, shape, conformation, and charge distribution of each molecular species in the system. It explicitly includes the conformations of the polymer and considers the acid-base equilibrium of each acid group of the polyelectrolyte.[38,39] Predictions of the molecular theory have been shown to be in excellent quantitative agreement with experimental observations for a variety of polymer related systems.[40–42] Relevant for current application, the prediction on the height of poly(acrylic acid) brushes in monovalent salt solutions were in good agreement with experimental observations.[43] Recently, we extended this molecular approach and developed a theoretical description of end-tethered weak polyelectrolytes in multivalent electrolyte solutions. Explicitly, we added the ability of calcium ions to bind with the polymer monomers, including the possibility to form calcium bridges. The binding of calcium to carboxylic acid monomers as well as the condensation of sodium ions are described via chemical equilibrium reactions. The binding constants describing these reactions are obtained from either simulations or experimental observations. Here, we shall present an outline of the molecular approach. Further details can be found in Ref.[37] as well as in the ESI†.

The basic idea of the molecular theory is to write the free energy of the system as a functional of the probability of the conformations of the polymer molecules and the spatial distribution of them. The minimization of the free energy determines the probability of each polymer conformation, the spatial distribution of the mobile species, and the chemical state of all species, depending on the value of the macroscopic variables such as pH, salt concentration, and temperature. The total free energy is given by

$$F = -TS_{conf} - TS_{mix} + E_{elect} + E_{VdW} + F_{chem}, \qquad (1)$$

where T is the temperature; S_{conf} is the conformational entropy of the tethered polymers chains; S_{mix} is the mixing (translational) entropy of the cations (Na^+ and Ca^{2+}), anions (Cl^-), water, pro-

tons, hydroxyl ions, and NaCl ion pairs. E_{elect} corresponds to the total electrostatic energy functional; E_{VdW} corresponds to non-electrostatic attractive Van der Waals interactions. F_{chem} is the free energy associated with the acid-base equilibrium of the acid monomers and the condensation or complexation of Ca^{2+} and Na^+ ions onto a deprotonated acid monomer. This free energy contribution describes the enthalpic and entropic cost associated with charging and uncharging of the acid groups of the poly acid, and the entropic and enthalpic cost associated with condensing Na^+ and Ca^{2+} ions to the charged acid group A^-. The steric repulsions between all molecular species are included separately as a constraint to the Helmholtz free energy. The system is assumed to be incompressible.

Based on the experimental evidence indicating that one calcium can bind with two acid monomers, we also include into the F_{chem} a free energy contribution that represents the possibility of forming calcium bridges or A_2Ca complexes. Explicitly, the acid-base and various ion condensation reactions are described by the following set of chemical equilibria

$$AH \rightleftharpoons A^- + H^+, \tag{2}$$

$$A^- + Na^+ \rightleftharpoons ANa, \tag{3}$$

$$A^- + Ca^{2+} \rightleftharpoons ACa^+, \tag{4}$$

$$2A^- + Ca^{2+} \rightleftharpoons A_2Ca. \tag{5}$$

Thus, we assume that the monomers can be found in one of the following five different states: protonated (AH), deprotonated (A^-), condensed with one sodium ion (ANa), or one calcium ion bound with either one or two charged acid monomers (ACa^+ and A_2Ca). We only consider complexes involving two acid monomers and one calcium ion. Larger complexes were not considered.

Each of the free energy terms is written as a functional of the density distribution of their molecular components and the probability distribution function of the polymer conformations. The distribution profiles, the probability of the different conformations, the electrostatic and repulsive position-dependent potentials, and the chemical state of each species are determined through the minimization of the total free energy. A detailed description of each of the terms of the free energy functional can be found in Ref.[37] and in the ESI†.

The input to the theory includes a very large set of unbiased polymer conformations, the bulk salt concentrations of NaCl and $CaCl_2$, the pH, the surface density of the end-tethered polymers and the radius and geometry of the surface (either spherical or cylindrical). Finally, the various dissociation equilibrium constants (pK's) of the acid-base chemical reaction (Eq. 2), the condensation reactions (Eqs. 4 and 3) , and calcium bridge formation (Eq. 5) in dilute solution are required. Their values were obtained from experiments and Molecular Dynamics simulations and are listed in the table 1. See Refs.[37,44] for further details.

The minimized free energy for each condition provides the probability of every polymer conformation, the chemical state (protonated, deprotonated, sodium or calcium condensed or a calcium bridged state) of every monomers, as well as the local densities of each of the different components and the local electrostatic potential.

Table 1 Dissociation Constants and standard reaction binding free energy $\Delta G_b^{\ominus}$ for acrylic acid (AA) monomers.

reaction	$pK(AA)$	$\Delta G_b^{\ominus}(AA)$ (kJ/mol)
$AH \rightleftharpoons A^- + H^+$	5.0	-38.5
$ANa \rightleftharpoons A^- + Na^+$	-0.40	-7.5
$ACa^+ \rightleftharpoons A^- + Ca^{2+}$	1.0	-15.7
$A_2Ca \rightleftharpoons 2A^- + Ca^{2+}$	4.0	-42.7

It is important to stress that in the systems studied, the molecular organization of the polymers and the ions, the physical interactions, and the chemical equilibria are strongly coupled. The molecular theory that we employed takes that coupling into account by solving in a self-consistent manner the probability of the chain conformations (polymer density), the chemical state of the monomers, the densities, the electrostatic potential and interactions fields appearing in the different free energy contributions. In this way, the chemical state of the monomer, meaning the fraction of (de)protonation, sodium and calcium condensation and calcium acid complexes, is not imposed but rather it is obtained as a result form the complex balance between the interactions in the system for the given conditions (pH, sodium and calcium concentration, surface geometry and radius). A further detailed description of the functional form of the free energy functional and each of its terms, the generation of chain conformations, and numerical procedure are presented in the supplementary information ESI† and in Ref.[37].

3 Results

In this section, we present and discuss a number of representative cases to illustrate the effect of curvature on the molecular organization and on the calcium-induced structural collapse of the polymer layer.

3.1 Structure of end-tethered pAA layers

Fig. 2 shows the polymer volume fraction profile of end-tethered pAA as a function of distance from the cylindrical surface. The figure illustrates the effect that both calcium ion and pH have on the structure of the polymer layer. The left panel corresponds to pH value of 3.0, whereas the right panel corresponds to a physiological value of 7.4. In both cases, the cylindrical nanoparticles have a radius of $R = 4$ nm and are end-tethered with poly(acrylic acid) polymers of 50 segments long with a polymer surface coverage of $\sigma = 0.15$ chains/nm^2. The modified nanoparticles are in contact with solutions that have different $CaCl_2$ concentrations, ranging from 0 to 10 mM (relevant for the extracellular environment)[45] but a fixed sodium chloride concentration corresponding to the physiological value of 150 mM.

For low pH values (pH = 3.0), we observe no influence of calcium ions on the structure of the polymer layer for the concentrations considered. Conversely, for physiological pH (7.4) we observe a strong structural response on adding calcium ions. Adding low amounts of divalent calcium ions ($c_{Ca^{2+}} \leq 0.1$ mM)

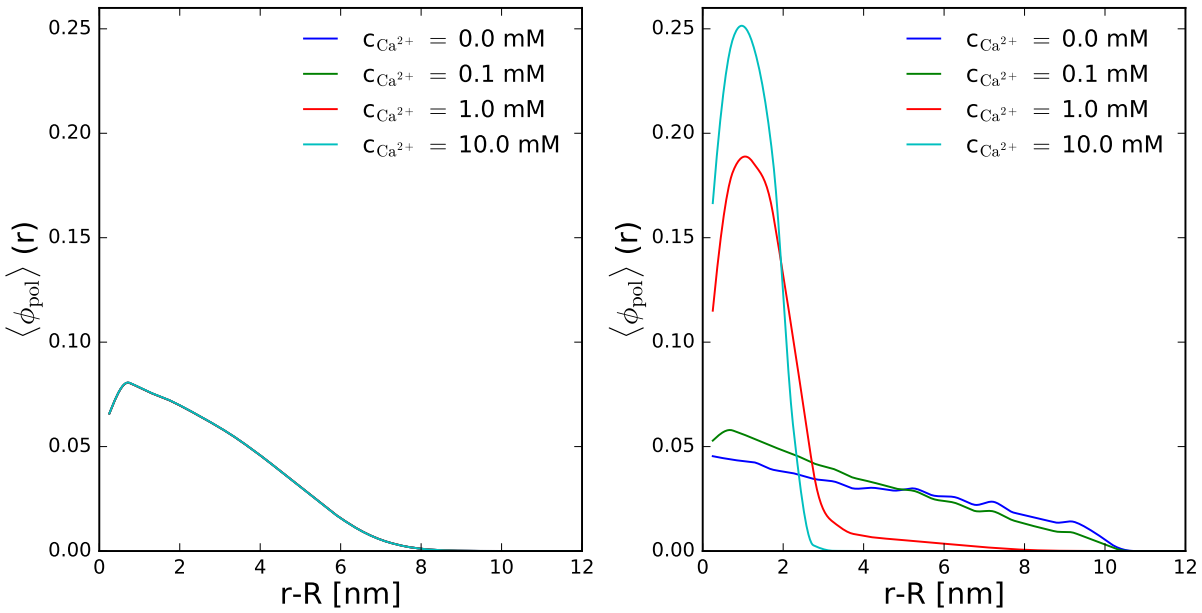

Fig. 2 The poly(acrylic acid) volume fraction as a function of the distance from the cylindrical surface for pH = 3.0 (left panel) and pH = 7.4 (right panel). The cylindrical nanoparticle has a radius of $R = 4$ nm. The lines correspond to different $CaCl_2$ concentrations, as indicated in the legend. The surface coverage is $\sigma = 0.15$ chains/nm^2. The polymer chain length or number of segments is $n = 50$. The bulk aqueous solution is characterized by NaCl concentration of 150 mM. The r-coordinate corresponds to the radial cylindrical coordinate used to describe the cylindrical symmetry of the NP.

does not result in noticeable structural changes for the polymers end-tethered to the cylindrical nanoparticle. The polymers form an extended, relative low density layer around the cylindrical nanoparticle. Increasing the concentration of calcium ions in the aqueous solution to values between 0.1 and 1.0 mM results in a rapid structural collapse of the polymer layer.

Qualitatively, this behavior can be understood as follows. At the low pH value of 3.0, the amount of deprotonated carboxylic monomers is very low and the polyelectrolyte layer is in a nearly uncharged, neutral state. Thus, the monomers do not (electrostatically) interact with the calcium ions and hence the structure is unaffected by the calcium concentration. However, with increasing pH the carboxylic acid groups deprotonate and become charged, resulting in electrostatic repulsions within the polymer layer. There are several strategies for the system to reduce these unfavorable electrostatic repulsions. First, the polymer chains can stretch further from the surface and from each other and the layer swells, as shown in the right panel of Fig. 3 for the case of zero added calcium ions (compare with left panel where chain are less stretched). However, chain stretching results in a loss of conformation entropy. Moreover, a polymer chain is only finite-extendable. Therefore, electrostatic repulsions cannot be mitigated by chain stretching alone. Besides chain stretching, another way to lower the electrostatic repulsions is to confine counter ions within the polymer layer, which leads to electrostatic screening. However, counterion confinement results in a reduction of the counterion translational entropy which, like chain stretching, is unfavorable. A third way to reduced the unfavorable electrostatic repulsions is charge regulation. Through shifting the acid-base equilibrium towards the protonated state the total amount of charge can be reduced. However, shifting the acid-base equilibrium to the uncharged state involves work against the chemical energy. So, the resulting amounts of charge and degree of swelling arise from a balance between the aforementioned forces. In the absence of calcium ions, this charge regulation mechanism leads to a reduction of the amount of charge within the layer. It should be noted that there are still charged carboxylic groups within the layer, albeit at a much lower degree as might have been expected based upon the pH of the solution (see Fig. S1 in the ESI†).

Now, when adding calcium ions other possibilities to regulate the amount of charge become feasible. Namely, calcium interacts strongly with carboxylic acid groups and can condense onto the deprotonated monomers. Not only that, calcium ions can form energetically favorable 'bridges', i.e., complexes of two acids and one calcium ion. The free energy gain associated with forming a calcium bridge is around $\Delta G_b^{\ominus} = -42$ kJ/mol (see Table 1). The formation of calcium bridges is energetically so favourable that the polymer layers will collapse if the solution contains high enough amount of calcium ions ($c_{Ca^{2+}} \geq 1.0$ mM in Fig. 3, right panel). In those systems, the loss of configuration entropy is compensated by the increases of the number of calcium bridges occurring due to the increased polymer density upon collapse. Due to formation of calcium bridges inside the layer the acids monomers are effectively neutralized and the effective charge of the polyelectrolyte layer drops (see Fig. S1 in the ESI† and also Ref.[37]). This reduction in total polymer charge reduces the number of counterions that need to be confined within the layer, enabling the release of otherwise confined counterions. This leads to a reduction in the loss of translation entropy of the counte-

rions, i.e., increased osmotic pressure, providing an extra thermodynamic driving force for the layer to collapse. To summarize, the weak polyelectrolyte layers of pAA will collapse under influence of calcium ions, beyond a certain threshold. The predicted collapse of end-tethered pAA is in agreement with past observations [18,19,22,25] on the collapse of planar and spherical pAA brushes and theoretical approaches [25,28,35,37].

3.2 Effect of surface curvature

To characterize and analyze in detail the role of curvature on the calcium induced collapse of the polymer layer it is convenient to consider the height of the polymer layer. The height corresponds to twice the first moment of the normalized r-dependent density of the monomers, $\langle \rho_p(r) \rangle$, minus the radius, R, of the nanoparticle:

$$h = 2\left(\langle r \rangle - R\right) \quad \text{with} \quad \langle r \rangle = \frac{\int_R^\infty r \langle \rho_p(r) \rangle G(r) \mathrm{d}r}{\int_R^\infty \langle \rho_p(r) \rangle G(r) \mathrm{d}r}. \tag{6}$$

The function $G(r)$ describes the change in volume as function of the distance away from the tethering surface. [39] Observe that we employed cylindrical and spherical coordinates to reflect the symmetry of the nanoparticles. Furthermore, the system is assumed to be laterally homogeneous and is only explicitly anisotropic in the radial direction r. Mathematically, the function $G(r)$ is the Jacobian determinant divided by the area of the surface: $G(r) = A(r)/A(R)$. [37,46] The height as defined above measures the thickness of the polymer layer and can be used to characterize the structure of the polyelectrolyte layer. From the height, we can determine whether the layer is swollen or collapsed.

Fig. 3 shows the height of a pAA layers end-tethered to cylindrical (top panel) and spherical (bottom panel) nanoparticles as a function of calcium concentration. The different lines in each panel correspond to different radii. We will start describing the behavior for the cylindrical nanoparticle with a radius of 4 nm. For such a system we observe that the height at low calcium concentrations is $h \approx 9.5$ nm, which corresponds to a swollen layer (see also the volume fraction profile in Fig. 2). Increasing the calcium concentration to the sub millimolar range leads to a relatively sharp decrease in the layer thickness, and around 1 to 2 mM, the layer thickness is reduced to $h \approx 2.5$ nm, which corresponds to a collapsed layer (also observed in Fig. 2). This behavior of the height versus calcium concentration is in line with the mechanism presented and discussed in the previous section.

Comparing the height versus calcium concentration for different radii shows a similar trend. However, as the radius increases, distinct changes in the size and shape of the thickness of the polymer layer as a function of calcium concentration can be observed. There are three aspects that are worth noting. First, increasing the radius of the nanoparticle at low calcium concentrations decreases the height of the swollen layer. Conversely, for high calcium concentrations ($c_{Ca^{2+}} \geq 1.0$ mM), the thickness of the collapsed layer increases with increasing radius. Second, if we define the transition concentration as the inflection point of the height curve, increasing the radius of the nanoparticle shifts the transition concentration at which the layer collapses to lower calcium concentrations. Third, the slope of the height versus calcium concentration curve at the transition concentration lowers with increasing surface radius. Thus, the transition region broadens, i.e., the concentration increase of calcium needed to collapse the brush increases, and the transition becomes less sharp.

Fig. 3 reflects how curvature modulates the molecular organization and the interplay between the different interactions acting in the system, such as steric, electrostatic, and chemical equilibria. Curvature effects encompass both changes in radius and changes in morphology (for example, spherical, cylindrical or planar surfaces). The differences are due to changes in the available volume as the distance from the surface increases, and with that, to changes in the steric repulsions in the system. For the case of planar surfaces, the available volume does not change

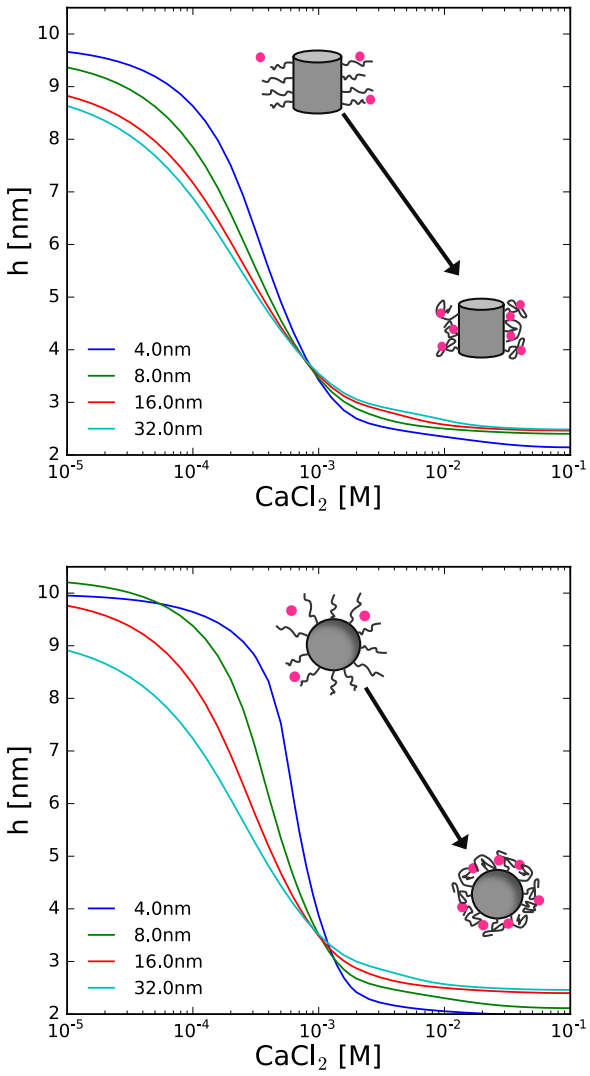

Fig. 3 The height of a poly(acrylic acid) end-tethered layer as a function of Ca^{2+} concentration for cylindrical nanoparticles (top panel) and spherical nanoparticles (bottom panel). The different lines correspond to different radii, as indicated in the legend. The pH of the solution and the amount of NaCl correspond to physiological conditions, 7.4 and 150 mM respectively. The surface coverage is $\sigma = 0.15$ chains/nm^2 and the number of segments is 50.

with increasing distance form the grafting surface. However, for curved spherical and cylindrical geometries, the available volume increases proportionally to $\propto r^2 dr$ and $\propto rdr$, respectively, where r corresponds to the radial spherical/cylindrical coordinate. The larger available volume as we move away from the surface for polymers grafted onto curved cylindrical or spherical surfaces translates into lower excluded volume repulsions. This modulates the way polymers end-tethered to that surface organize in space.[46–49] For example, neutral polymers layers grafted to a planar surface form a 'parabolic' shaped polymer density profile, whereas the profile of cylindrical end-tethered layers has a 'exponential' decaying shape.[39,46]

For end-tethered charged polyelectrolytes the impact of surface curvature is further amplified, given the electrostatic repulsions within the polymer layer. Also, the chemical equilibria present in the system (acid-base, ion condensation, and complex formation, Eqs. 2, 3, 4, and 5) are directly affected with the surface curvature. In absence of calcium ions, the charge regulation mechanism[13,39,50], outlined in the previous section, shifts the acid-base chemical equilibrium to the protonated, uncharged state of the acid monomers. The more compact the polymer layer (the higher the polymer density), the larger the shift in order to regulate the amount of charges down. In the presence of calcium ions, the free energy balance changes and critically dependents on the possibility to form calcium bridges. For a calcium concentration of $c_{Ca^{2+}} = 0.1\,\text{mM}$, the average fraction of calcium bridges for $R = 4, 8, 16\,\text{nm}$ equals $\langle f_{A_2Ca} \rangle = 0.17, 0.24, 0.30$ respectively (see Fig. S2 ESI†). Thus, with increasing radius the amount of calcium bridges increases. Because the monomer density is higher for lower curved surfaces (higher radius), it becomes 'easier' to form calcium bridges at lower calcium concentrations, driving the reduction of the height of the layer. However, at the same time, the larger polymer density leads to an increase in the excluded volume interactions, which prevents an immediate collapse of the layer and a larger transition region occurs. At high calcium concentrations, there are sufficient calcium ions to from enough calcium bridges to energetically overcome the loss of conformational entropy and excluded volume interactions and the layers collapses independently of radius. The thickness of the collapsed state increases with decreasing curvature (higher radius) since the number of monomers per volume increases.

The bottom panel of Fig. 3 shows results pertaining to spherical nanoparticles. Polymers end-tethered to spherical surfaces show a qualitatively similar behavior as cylindrical surfaces, but they behave quantitatively different. For example, at a calcium concentration of $0.1\,\text{mM}$, the thickness of polymer layer end-grafted to cylindrical nanoparticle with a radius of $R = 4\,\text{nm}$ is already significantly reduced and partially collapsed. On the other hand, the polymer layer end-tethered to a spherical nanoparticle of radius $R = 4\,\text{nm}$ is in a swollen state. This difference in behavior is also reflected in the fraction of acid monomers that form calcium bridges. Comparison between cylindrical and spherical nanoparticles for identical solution and grafting conditions as well as radius, shows that the average fraction of calcium bridges is much lower for the spherical nanoparticle (see Fig. S2 ESI†). This difference can be understood in terms of the volume argument discussed above. Namely, the increase in available volume away from a spherical surface is larger than for a cylindrical surface. Consequently, for the same surface density of polymers, the monomers grafted to a spherical nanoparticle will have more available volume away from the surface. Hence, the monomer number density will be lower for polymer attached to a sphere than to a cylinder. Since the polymer density is lower, the number of calcium bridges will be lower as well and there is a smaller thermodynamic driving force to collapse. However, the lower polymer density also reduces the amount of steric repulsions, and once sufficient calcium ions are present, the layer will be able to collapse more 'easily'. This explains the more abrupt transition for a spherical surface as compared to a cylindrical one of the same radius.

The interplay of surface curvature and the interactions present in the system is summarized in Fig. 4, showing the thickness of the end-tethered layer as a function of radius for cylindrical and spherical nanoparticles. The figure also emphasizes the large effect that calcium concentration has one the layer thickness and stress the quantitative difference between spherical and cylindrical surfaces. Qualitatively, at low calcium concentration, the swollen state contracts and the thickness decreases with increasing radius for both cylindrical and spherical nanoparticles. In spite of this overall decrease in polymer layer height with radius, we also observe non-monotonic changes of the thickness as function of radius at these lower calcium concentrations. These are partially consequence of numerical noise and the way the polymer conformations are sampled in the theory. In such conditions, the layers are in a swollen, extended state and the thickness is primarily determined by the distal region of the polymer volume fraction profile. Hence, small changes in the distal part of the density profile can have a large effect on the polymer layer height (see Eq. 6). The extended polymer conformations that are favored in these conditions might be not sufficiently sampled. However, increasing the size of the sample or decreasing the discretization step, even though it reduced the inaccuracy and corrugation of the density, it did not remove it. This stresses that the most important factor behind this non-monotonic behavior is the non-trivial and complex balance between the various chemical and physical interactions that determine the molecular organization of the layer. At higher calcium concentrations, for which the polymer layer has collapsed ($c_{Ca^{2+}} \geq 1.0\,\text{mM}$), the behavior reverses and the thickness of the now collapsed layer slightly increases. Note, however, the differences between the spherical and cylindrical systems for radii $\leq 10\text{nm}$ and calcium concentration $1.0\,\text{mM}$. This again emphasizes the non-trivial effect of curvature, and how it modulates all interactions present in the system.

3.3 Thermodynamic behavior

In this section we expand on the structural information provided by the height-curve of Fig. 3 to show the corresponding thermodynamic properties for these two systems by presenting the chemical potential of the tethered polymer. The chemical potential gives insight into the interactions at play and provides information about the thermodynamic stability of the polymer layer.

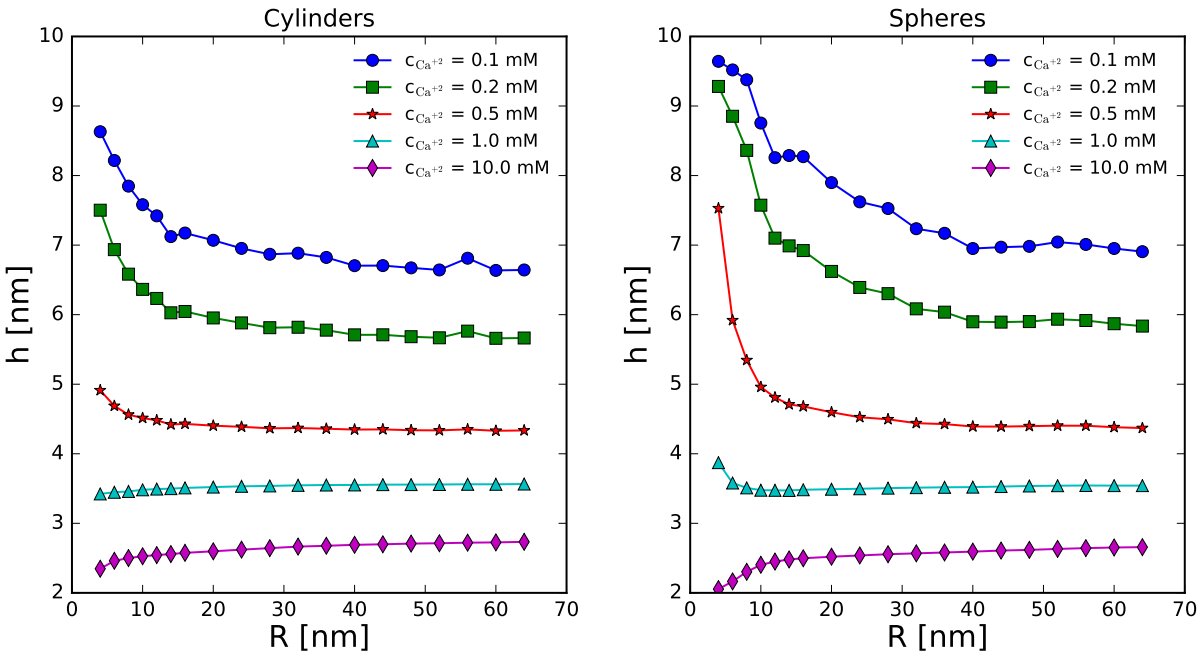

Fig. 4 The height of the end-tethered poly(acrylic acid) layer as a function of the radius for cylindrical nanoparticles (left panel) and spherical nanoparticles (right panel) The different lines correspond to different calcium concentration. The pH is equal to 7.4 and the NaCl concentration is 150 mM. The surface coverage is $\sigma = 0.15$ chains/nm^2, and the number of segments is 50.

From the chemical potential in Fig. 5, we observe that the chemical potential monotonically decreases as a function of the calcium concentration and displays two distinct regions, that correlate with the swollen and collapsed state of the polymer layer (Figs. 2 and 3). The thermodynamics of the system arises from a non-trivial balance between various opposing forces: conformation entropy of the chains, counterion confinement, electrostatic and exclude volume repulsions. For low calcium concentrations, in the range of $10^{-5} - 10^{-4}$ molar, we observe a relative small change in the chemical potential to an increase in the calcium concentration for all radii studied. For these conditions, the effect of calcium bridges is less important and the chemical potential is less 'sensitive' to changes in the calcium ion concentration. Note however, that in this region curvature plays and important role. The increasing chemical potential with increasing radii is a consequence of the increase in steric repulsions. Now, for $c_{Ca^{2+}} > 0.5$ mM the shape of the chemical potential changes and shows an almost linear decrease with increasing amounts of calcium ions. This is because at these higher calcium concentrations the formation of calcium bridges dominates over the other interactions in the system. With increasing calcium ions more calcium bridges occur and the free energy and chemical potential will decrease in an almost linear fashion. It is worth noting that the calcium concentrations at which this 'linear' region starts correspond roughly to the transition points discussed in Fig. 3. The behavior is most prominently visible for the small spherical nanoparticle, whose collapse behavior is most abrupt. cf. Fig. 5 with Fig. 2. The shape of the chemical potential confirms and underpins the importance of calcium concentration in the collapse of the polyelectrolyte layer and emphasizes the role of curvature, as discussed in the previous sections.

To analyze the thermodynamic stability of the layer, we studied the chemical potential of the polymer layer as a function of the surface coverage (the number of polymers per unit area). Results are presented in Fig. 6. The different lines correspond to different calcium concentrations, which are in the range of physiological extracellular concentrations.[45] At a first glance, comparing the chemical potential of the spheres and cylinders large qualitative differences are evident. We observe that for calcium concentrations < 1.0 mM the chemical potential monotonically increases. The positive slope of the chemical potential indicates a thermodynamically stable system. For increasing calcium concentrations in this range, the chemical potential is still monotonically increasing but the positive slope becomes smaller. Increasing the calcium concentration further, the chemical potential attains a negative slope for both cylindrical and spherical nanoparticles. Notice the non-monotonic behavior of the chemical potential of the spherical nanoparticle at $c_{Ca^{2+}} = 1.0$ mM. Such feature was not observed for the cylindrical nanoparticle at the same conditions. The negative slope and non-monotonic behavior occur for those conditions where the polymer layer transitions from a swollen to a collapsed state (see Fig. 3). This change from monotonic increasing chemical potential to a chemical potential with either a negative slope or non-monotonic change suggests the possibility for phase separation. However, since in our calculations the polymers are irreversibly end-tethered to the surface and do not have translational degrees of freedom to move, this cannot result in a macroscopic phase separation between two macroscopic phases.[51,52] In turn, the non-monotonic behavior indicates the potential for domain formation or microphase separation in the lateral direction

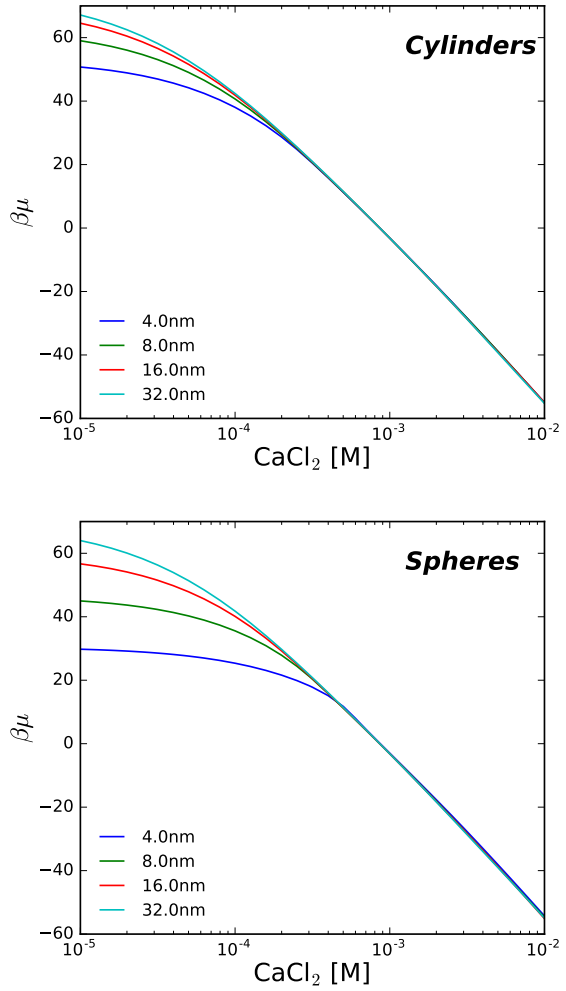

Fig. 5 Chemical potential of end-tethered poly(acrylic acid) as a function of calcium concentration for cylindrical (top panel) and spherical nanoparticles (bottom panel). The different lines correspond to different radii. The pH is equal to 7.4 and the NaCl concentration is 150 mM. The surface coverage is $\sigma = 0.15$ chains/nm^2, and the number of segments is 50.

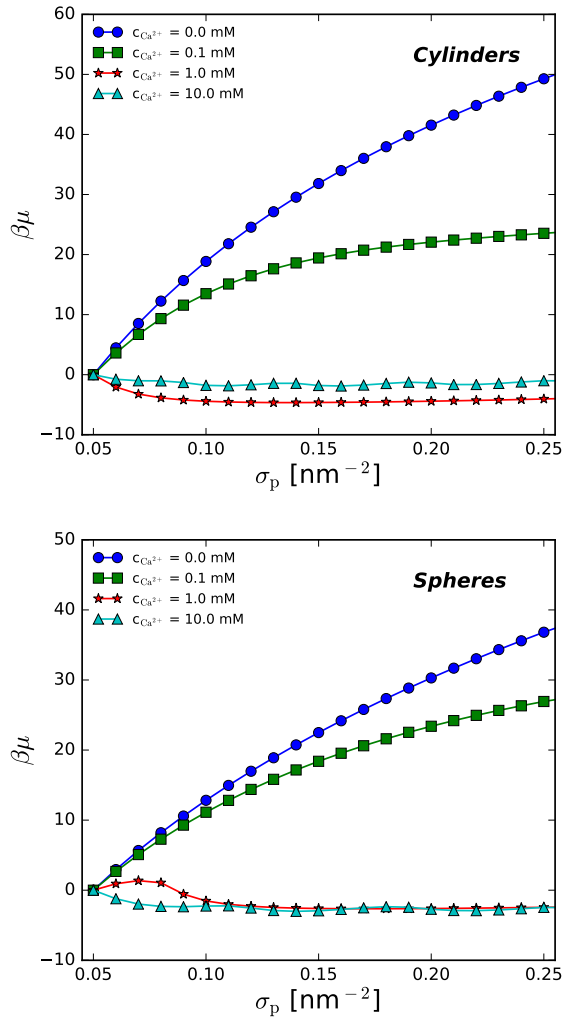

Fig. 6 Chemical potential of end-tethered poly(acrylic acid) as function of number of chains per unit area or surface coverage. The top panel corresponds to a cylindrical nanoparticle whereas the bottom panel represents a spherical nanoparticle. The different lines correspond to different calcium concentrations. The pH is equal to 7.4 and the NaCl concentration is 150 mM. The radius of the nanparticle is equal to $R = 4$ nm and the number of segments is 50. The chemical potential curves where shifted such that at $\sigma_p = 0.05 nm^{-2}$ the chemical potential is zero for each condition.

of the collapsed layer.[53,54] The notion of microphase separation is also suggested by the observation that for the case of the non-monotonical behavior of the chemical potential for the spherical nanoparticle at $c_{Ca^{2+}} = 1.0$ mM, the structural organization drastically changes as function of surface density (see Fig. S3 of ESI†). For low grafting densities the layer is a swollen state, while for higher surface density it transitions towards a collapsed state (see Fig. S3 of ESI†). It can be envisioned that this could lead to lateral polymer density variations, resulting in e.g., local domains similar to the ones observed for weak polyelectrolytes grafted to planar surfaces.[54] To investigate the possibility of structure formation in the lateral directions, further 2D or 3D calculations are required. Noteworthy in this respect, is that recent work by Pincus and coworkers utilizing theory[28] and MD simulations[36] to study grafted strong polyelectrolytes in multivalent (trivalent) ion solutions also showed the possibility to form lateral heterogeneous planar brushes.

4 Summary and Concluding Remarks

In this work we have investigated the interplay between nanoparticle surface curvature and morphology on the calcium binding to end-tethered poly(acrylic acid) layers, under physiological pH and monovalent NaCl concentrations. A recently developed molecular theory that describes the properties of weakly chargeable grafted polyelectrolytes in multivalent ion solutions was employed. We presented and rationalized the molecular organization and the structural changes of cylindrical and spherical end-tethered polyelectrolytes in response to variations in calcium concentrations. We found calcium binding to be not only controlled by the calcium ion concentration but also strongly influenced by the curvature of the grafting surface. The polymer layers collapsed in aqueous solutions that contain sufficient amounts of

Ca^{2+} ions, due to the formation of calcium bridges. The transition from a swollen to a collapsed layer as function of calcium concentration broadens and shifts to lower calcium concentrations as function of radius for cylinders and spheres.

The dependence of the collapse transition of the polymer layer on curvature and geometry emphasizes the strong and non-trivial coupling between molecular organization, and the physical and chemical interactions acting in the system. These results are particularly relevant for engineering modified nanoparticles for biological environments, in which calcium concentrations change in the range from nanomolar to micromolar (for cytoplasm and extracellular surrounding, respectively). Also, the size (radius) and shape (spherical versus cylindrical nanofibers) selected for the nanoparticle have been shown to have non-trivial effects on the behavior of the nano-construct in environments with different calcium concentrations. This has implications for nanoparticle stability, drug delivery strategies, and the design of nanomaterials responsive to calcium ions. Moreover, a comprehensive understanding of the formation of calcium bridges between weak polyelectrolyte chains grafted to curved geometries would also contribute to rational design and optimization of smart interfaces with applications in, e.g., salt-sensitive and ion-responsive materials and devices.

The molecular theory used in this work was explicitly developed to describe the calcium ion binding to tethered weak polyelectrolytes with carboxilic acid groups.[37] This basic framework sets the stage for potential new directions of investigation. For example, given its strong interactions with DNA molecules, Mg^{2+} ions could be considered instead of Ca^{2+}. Another research direction can involve a more thorough exploration of the possible microphase separation discussed in the previous section, by performing 2D or 3D calculations. Also, the collapse of the tethered layer is suggestive that the interactions between polymer coated nanoparticles could shift from repulsive to attractive in multivalent ion solutions, leading to aggregation. With the molecular theory presented in this work, the interactions between modified nanoparticles could be studied[54–56], shedding light on the dispersion stability of tethered nanoparticles in multivalent ion solutions. Given the growing interest in engineering the nano-bio interface, such understanding of dispersion stability becomes key. Also, the theoretical framework presented here can be extended to study the adsorption of poly(acrylic acid) onto surfaces of different geometry,[57] to understand the relevant synthesis conditions in which nanosystems as the ones studied in this work could be obtained. Extensive computer simulations have been recently performed studying the adsorption of PA chains onto charged surfaces.[58,59] In such scenarios, the molecular theory can provide a deeper molecular understanding of the interactions between polyelectrolytes in multivalent ions solutions, which is fundamental for a rational design of nanomaterials with applications in biological environments.

Conflict of interest

The authors declare no conflict of interest.

Acknowledgement

R.J.N. and I.S. acknowledge research support as part of the Center for Bio-Inspired Energy Science, an Energy Frontier Research Center funded by the U.S. Department of Energy (DOE), Office of Science, Basic Energy Sciences (BES), under Award # DE-SC0000989. E.G.S. and I.S. acknowledge support from Grant No.EB005772 from the National Institute of Biomedical Imaging and Bio-engineering (NIBIB). This research was supported in part through the computational resources and staff contributions provided for the Quest high performance computing facility at Northwestern University which is jointly supported by the Office of the Provost, the Office for Research, and Northwestern University Information Technology.

The authors would like to thank Dr. Kai Huang for carefully reading the manuscript.

References

1 D. E. Clapham, *Cell*, 2007, **131**, 1047–1058.
2 M. P. Mattson and S. L. Chan, *Nat. Cell Biol.*, 2003, **5**, 1041–1043.
3 A. G. Szent-Györgyi, *Bio. Phys. J.*, 1975, **15**, 707–723.
4 R. Phengchat, H. Takata, K. Morii, N. Inada, H. Murakoshi, S. Uchiyama and K. Fukui, *Sci. Rep.*, 2016, 1–10.
5 M. Brini, T. Calì, D. Ottolini and E. Carafoli, *Cell. Mol. Life Sci.*, 2014, **71**, 2787–2814.
6 N. K. Dhami, M. S. Reddy and A. Mukherjee, *Front. Microbiol.*, 2013, 1–13.
7 A. K. Gupta and M. Gupta, *Biomaterials*, 2005, **26**, 3995–4021.
8 W. Senaratne, L. Andruzzi and C. K. Ober, *Biomacromolecules*, 2005, **6**, 2427–2448.
9 B. Jeong and A. Gutowska, *Trends in biotechn.*, 2002, **20**, 305–311.
10 C. de las Heras Alarcón, S. Pennadam and C. Alexander, *Chem. Soc. Rev.*, 2005, **34**, 276–285.
11 P. Pincus, *Macromolecules*, 1991, **24**, 2912 – 2919.
12 E. B. Zhulina, O. V. Borisov and T. M. Birshtein, *J. Phys. II Fr.*, 1992, **2**, 63–74.
13 R. Israëls, F. A. M. Leermakers and G. J. Fleer, *Macromolecules*, 1994, **27**, 3087–3093.
14 R. Israëls, F. A. M. Leermakers, G. J. Fleer and E. B. Zhulina, *Macromolecules*, 1994, **27**, 3249 – 3261.
15 E. B. Zhulina, T. M. Birshtein and O. V. Borisov, *Macromolecules*, 1995, **28**, 1491.
16 A. A. Mercurieva, T. M. Birshtein, E. B. Zhulina, P. Iakovlev, J. van Male and F. A. M. Leermakers, *Macromolecules*, 2002, **35**, 4739 – 4752.
17 E. B. Zhulina and O. V. Borisov, *Langmuir*, 2011, **27**, 10615–10633.
18 A. Ezhova and K. Huber, *Macromolecules*, 2016, **49**, 7460–7468.
19 R. Konradi and J. Rühe, *Macromolecules*, 2005, **38**, 4345–4354.
20 Y. Mei and M. Ballauff, *Eur. Phys. J. E*, 2005, **16**, 341–349.

21 Y. Mei, K. Lauterbach, M. Hoffmann, O. V. Borisov, M. Ballauff and A. Jusufi, *Phys. Rev. Lett.*, 2006, **95**, 158301.

22 R. Farina, N. Laugel, P. Pincus and M. Tirrell, *Soft Matter*, 2013, **9**, 10458–10472.

23 C. Schneider, A. Jusufi, R. Farina, P. Pincus, M. Tirrell and M. Ballauff, *Phys. Rev. E*, 2010, **82**, 011401.

24 J. Yu, J. Mao, G. Yuan, S. Satija, W. Chen and M. Tirrell, *Polymer*, 2016, **98**, 448–53.

25 J. Yu, N. E. Jackson, X. Xu, B. K. Brettmann, M. Ruths, J. J. de Pablo and M. Tirrell, *Sci. Adv.*, 2017, **3**, 1–10.

26 J. Rühe, M. Ballauff, M. Biesalski, P. Dziezok, F. Gröhn, D. Johannsmann, N. Houbenov, N. Hugenberg, R. Konradi, S. Minko, M. Motornov, R. R. Netz, M. Schmidt, C. Seidel, M. Stamm, T. Stephan, D. Usov and H. Zhang, *Adv. Polym. Sci.*, 2004, **165**, 79–150.

27 M. Ballauff, *Progress in Polymer Science*, 2007, **32**, 1135–1151.

28 B. Brettmann, P. Pincus and M. Tirrell, *Macromolecules*, 2017, **50**, 1225–1235.

29 B. K. Brettmann, N. Laugel, N. Hoffmann, P. Pincus and M. Tirrell, *J. Polym. Sci., Part A: Polym. Chem.*, 2015, **54**, 284–291.

30 T. Jiang and J. Wu, *J. Chem. Phys.*, 2008, **129**, 084903.

31 T. Jiang and J. Wu, *J. Phys. Chem. B*, 2008, **112**, 7713–7720.

32 Q. Cao, C. Zuo, L. Li and H. He, *Modelling Simul. Mater. Sci. Eng.*, 2010, **18**, 075001.

33 Q. Cao, C. Zuo, H. He and L. Li, *Macromol. Theory Simul.*, 2009, **18**, 441–452.

34 Y. Mei, M. Hoffmann, M. Ballauff and A. Jusufi, *Phys. Rev. E*, 2008, **77**, 031805.

35 N. E. Jackson, B. K. Brettmann, V. Vishwanath, M. Tirrell and J. J. de Pablo, *ACS Macro Letters*, 2017, 155–160.

36 L. Liu, P. A. Pincus and C. Hyeon, *Macromolecules*, 2017, **50**, 1579–1588.

37 R. J. Nap, S. H. Park and I. Szleifer, *Soft Matter*, 2018, accepted for publication, doi: 10.1039/C7SM02434G.

38 I. Szleifer and M. A. Carignano, *Adv. Chem. Phys.*, 1996, **94**, 165–260.

39 R. Nap, P. Gong and I. Szleifer, *J. Polym. Sci., Part B: Polym. Phys.*, 2006, **44**, 2638–2662.

40 G. S. Longo, D. H. Thompson and I. Szleifer, *Langmuir*, 2008, **24**, 10324 – 10333.

41 D. Wang, R. J. Nap, I. Lagzi, B. Kowalczyk, S. Han, B. A. Grzybowski and I. Szleifer, *J. Am. Chem. Soc.*, 2011, **133**, 2192–2197.

42 M. Tagliazucchi, O. Azzaroni and I. Szleifer, *J. Am. Chem. Soc.*, 2010, **132**, 12404–12411.

43 P. Gong, T. Wu, J. Genzer and I. Szleifer, *Macromolecules*, 2007, **40**, 8765–8773.

44 S. H. Park, R. J. Nap and I. Szleifer, *ArXiv e-prints*, 2018, arXiv:1801.05888[physics.chem–ph].

45 K. Wójcik-Piotrowicz, J. Kaszuba-Zwoińska, E. Rokita and P. Thor, *Prog. Biophys. Mol. Biol.*, 2016, **121**, 45 – 53.

46 M. A. Carignano and I. Szleifer, *J. Chem. Phys.*, 1995, **102**, 8662–8669.

47 S. Misra, W. Mattice and D. H. Napper, *Macromolecules*, 1994, **27**, 7090 – 7098.

48 R. C. Ball, J. F. Marko, S. T. Milner and T. A. Witten, *Macromolecules*, 1991, **24**, 693–703.

49 M. Murat and G. S. Grest, *Macromolecules*, 1991, **24**, 704–708.

50 R. J. Nap, M. Tagliazucchi and I. Szleifer, *J. Chem. Phys.*, 2014, **140**, 024910.

51 M. A. Carignano and I. Szleifer, *J. Chem. Phys.*, 1994, **100**, 3210–3223.

52 P. Gong, J. Genzer and I. Szleifer, *Phys. Rev. Lett.*, 2007, **98**, 018302.

53 O. Peleg, M. Tagliazucchi, M. Kröger, Y. Rabin and I. Szleifer, *ACS Nano*, 2011, **5**, 4737–4747.

54 M. Tagliazucchi, M. Olvera de la Cruz and I. Szleifer, *Proc. Natl. Acad. Sci. U.S.A.*, 2010, **107**, 5300.

55 R. J. Nap, S. H. Park and I. Szleifer, *J. Polym. Sci., Part B: Polym. Phys.*, 2014, **52**, 1689–1699.

56 K. Huang and I. Szleifer, *J. Am. Chem. Soc.*, 2017, **139**, 6422–6430.

57 E. Gonzalez Solveyra, M. Tagliazucchi and I. Szleifer, *Faraday Discuss.*, 2016, **191**, 351–372.

58 D. L. Z. Caetano, S. J. de Carvalho, R. Metzler and A. G. Cherstvy, *Phys. Chem. Chem. Phys.*, 2017, **19**, 23397–23413.

59 S. J. d. Carvalho, R. Metzler and A. G. Cherstvy, *New J. Phys.*, 2016, **18**, 083037.

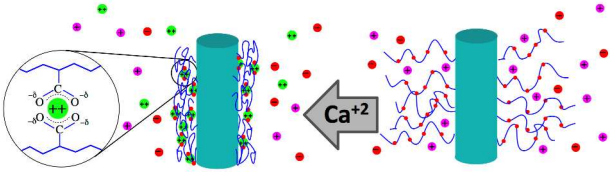

Calcium binding and surface curvature determine the structural and functional properties of weak polyelectrolytes grafted to nanoparticles in biological environments